Translational Oncology 21 (2022) 101424

Contents lists available at ScienceDirect

Translational Oncology

journal homepage: www.elsevier.com/locate/tranon

Original Research

A novel multifunctional anti-PD-L1-CD16a-IL15 induces potent cancer cell killing in PD-L1-positive tumour cells

Yumei Li [a], Lingjun Wu [a], Yueying Liu [b], Siwen Ma [a], Biyi Huang [a], Xianjing Feng [a,*], Hui Wang [a,*]

[a] School of Pharmacy, Guangxi Medical University, Nanning, China
[b] Department of Hypertension, The First Affiliated Hospital of Guangxi Medical University, Nanning, China

ARTICLE INFO

Keywords:
Single domain antibody
Phage display
PD-L1
IL15/IL-15Ra
CD16a
HEK-293F

ABSTRACT

Cancer is the most acute disease and the leading cause of patient death worldwide. Both chemotherapy and molecular-based therapies play an important role in curing cancer. However, the median and overall survival of patients is poor. To date, immune therapies have changed the treatment methods for cancer patients. Programmed death ligand 1 (PD-L1, also known as B-H1, CD274) is a well-studied tumor antigen. PD-L1 is overexpressed in colon cancer, lung cancer, and so on and plays a vital role in cancer development. In this study, anti-PD-L1 single-domain antibodies were identified from recombinant human PD-L1 (rhPD-L1)-immunized llamas. Then, we generated a novel multifunctional anti-PD-L1-CD16a-IL15 antibody targeting PD-L1-positive tumor cells. Anti-PD-L1-CD16a-IL15 was constructed by linking the Interleukin-2 (IL-2) signal peptide, anti-PD-L1 single domain antibody (anti-PD-L1-VHH) and anti-cluster of differentiation 16a single domain antibody (anti-CD16a-VHH), and Interleukin-15/Interleukin-15 receptor alpha (IL15/IL-15Rα). This anti-PD-L1-CD16a-IL15 fusion protein can be expressed and purified from HEK-293F cells. *In vitro*, our data showed that the anti-PD-L1-CD16a-IL15 fusion protein can recruit T cells and drive natural killer cells (NK) with specific killing of PD-L1-overexpressing tumor cells. Furthermore, in the xenograft model, the anti-PD-L1-CD16a-IL15 fusion protein inhibited tumor growth with human peripheral blood mononuclear cells (PBMCs). These data suggested that the anti-PD-L1-CD16a-IL15 fusion protein has a latent function in antitumour activity, with better guidance for future cancer immunotherapy.

Introduction

Cytokines are a broad and loose category of small proteins (~5–20 kDa). Cytokines are essential mediators of communication for the human immune system, and a number of them are crucial for host defense against pathogens [1]. To date, an increasing number of studies have focused on applying many types of cytokines in antiviruses and cancer treatment [2]. Among cytokines, IL-15 has been listed as the most promising antitumor drug candidate [3]. IL-15 and IL-2 belong to the same cytokine family [4], IL-15 and IL-2 have the same receptor β chain and γ chain (IL-2/15βγ), but they have different α receptor chains Interleukin-2 receptor alpha/ Interleukin-15 receptor alpha (IL-2Rα/IL-15Rα) [5]. Similar to IL-2, IL-15 can stimulate the proliferation of T cells and natural killer (NK) cells, the expansion of cytotoxic T cells [6], and the activation of NK cells [7]. However, IL-2 but not IL-15 has immunosuppressive effects [5]. IL-15 may have more potent antitumor activity than IL-2. Interestingly, the IL-15/IL-15Rα complex increases the activity of IL-15 by approximately 50 times [8]. Therefore, an IL-15/IL-15Rα fusion protein may perform better than IL-15 alone. Given the multiple functions of IL-15, including increasing the number of activated natural killer (NK) cells, monocytes, and granulocytes, a systemic increase in IL-15 activity may lead to high toxicity [9,10]. Recombinant IL-15 has been used in clinical research for cancer treatment, but its efficacy is limited due to its half-life and toxicity [10]. Therefore, targeting IL-15 to the tumor microenvironment, allowing immune cells to specifically participate in the tumor microenvironment to enhance the antitumor effects of IL-15, will be an attractive strategy. IL-15 activates NK cells, and antibody-dependent cellular cytotoxicity (ADCC) is one of the main cytotoxic mechanisms by which FcγR-expressing effector cells eliminate tumor cells. It has been reported that a bispecific antibody modified the IL-15 crosslinker through genetic insertion to enhance ADCC and activate NK cells to improve anticancer efficacy [11]. In addition, targeting the CLEC12A trispecific killer conjugation molecule can effectively induce NK cells to improve the

* Corresponding authors.
E-mail addresses: feng.xianjing@qq.com (X. Feng), wanghui@gxmu.edu.cn (H. Wang).

https://doi.org/10.1016/j.tranon.2022.101424
Received 26 January 2022; Received in revised form 3 April 2022; Accepted 6 April 2022
Available online 26 April 2022
1936-5233/© 2022 Published by Elsevier Inc. This is an open access article under the CC BY-NC-ND license (http://creativecommons.org/licenses/by-nc-nd/4.0/).

efficacy against AML tumors [12]. On the other hand, by increasing IL-15-mediated activation of CD8 T cells, a tumor microenvironment targeting IL-15 using RGD or CEA was constructed and shown to exhibit strong antitumor activity [13,14].

CD16 (FcγRIII), a receptor for the IgG Fc domain, FcγRIIIa (CD16a) and FcγRIIIb (CD16b), facilitates ADCC and plays an essential role in triggering the lysis of target cells by natural killer (NK) cells [15]. It has been shown that monocytes expressing CD16 have a variety of ADCC capabilities in the presence of specific antibodies and can kill cancer cells [16]. Furthermore, CD16a is a potent cytotoxicity receptor on human NK cells, which can be exploited by therapeutic bispecific antibodies [17]. Human NK cells account for ~10% of all lymphocytes and are defined phenotypically by the expression of cluster of differentiation 56/cluster of differentiation 16 (CD56+CD16+) [15]. Two isoforms of human CD16, CD16a and CD16b, share 96% sequence identity in their immunoglobulin-binding regions. CD16a is expressed on NK cells, macrophages, and mast cells and is an activating receptor [18]. On the other hand, CD16b is expressed on granulocytes as a GPI-anchored receptor and does not lead to tumor cell killing [18]. Bispecific antibodies are attractive candidates for cancer immunotherapy because they can effectively induce NK cells to kill tumor cells [16]. To activate NK cells, anti-CD16a antibodies have been studied and used to develop bispecific antibodies [16,17].

Programmed death-ligand 1 (PD-L1), also known as cluster of differentiation 274 (CD274) or B7 homologue 1 (B7-H1), is a protein that in humans is encoded by CD274 gene [19,20]. PD-L1 overexpression occurs in different kinds of human cancers, including colon [21], lung [22], pancreas [23], breast [24], ovarian [25], and head and neck cancers [26]. The overexpression of PD-L1 leads to tumor cell progression and tumorigenesis [27]. The tumor microenvironment plays an important role in good prognosis in immunotherapy based on programmed death-ligand 1/programmed cell death protein 1/cluster of differentiation 80 (PD-L1/PD-1/CD80) immune checkpoint inhibitors [28]. Durvalumab is an FDA-approved anti-PD-L1 monoclonal antibody (mAb) for immune checkpoint blockers in patients with lung adenocarcinoma [29]. However, although immune checkpoint inhibitors show great clinical benefits, their efficacy is still modest [30]. To date, there is no benefit against PD-L1-positive colon cancer. Thus, it is better to develop new ways to improve PD-L1-targeting cancer therapy.

Studies have shown that an attractive strategy to improve the antitumor effect of antibodies is to use smaller antibody formats to increase tumor penetration [31]. Many mAb fragments, such as antigen-binding fragment (Fab), single-chain variable fragment (scFv), and nanobodies, have been widely used. However, Fabs and scFvs have low yields, poor stability and solubility, and short half-lives *in vivo* [9]. Single domain antibodies, also called nanobodies or single domain antibody (VHH), are derived from the variable domains of heavy-chain antibodies in camelids [32]. Although VHH is the smallest fully functional antigen-binding fragment (approximately 15 kDa), its specificity and affinity for recognizing antigens are similar to those of immunoglobulin G (IgG) antibodies [33]. Due to its smaller size, VHH has enhanced tissue penetration and epitope entry [33]. In addition, single-domain antibodies can be expressed in high yields, and VHH also exhibits high thermal stability, conformational stability, and solubility and is resistant to acids and alkalis [34,35]. These excellent characteristics make VHH a valuable and attractive tool for various applications.

Phage display technology has been used to screen and identify ligands for proteins and other molecules, select peptides and antibodies, improve peptide or antibody affinity, and indicate protein–protein interactions [36,37]. In addition, bacteriophage lambda, representing a classical cloning and expression system, can express peptide or protein sequences as fusions to coat proteins [38]. More recently, whole-genome bacteriophage lambda display human libraries are a relatively novel use for identifying new antigens for biomedical applications [39,40].

This study constructed an anti-PD-L1-CD16a construct by fusing an anti-PD-L1 VHH with an anti-CD16a VHH. Another anti-PD-L1-IL15 construct functions by fusing an anti-PD-L1 VHH with IL-15/IL-15Ra. A novel multifunctional anti-PD-L1-CD16a-IL15 antibody was constructed by linking anti-PD-L1-VHH and anti-CD16a-VHH antibodies and IL-15/IL-15Ra. All these fusion proteins can promote immune cell proliferation to drive potent PD-L1-positive tumor cell killing *in vitro* and *in vivo*. In addition, compared with anti-PD-L1-CD16a or anti-PD-L1-IL15, anti-PD-L1-CD16a-IL15 showed better activity. These findings hold significant importance for using anti-PD-L1-CD16a-IL15 as a potential cancer immunotherapy.

Materials and methods

Immunized VHH phage display library construction

PD-L1 single domain antibodies were generated as described previously [41]. Second, recombinant human PD-L1-His-protein (Genscript) was used to immunize llamas. Third, the serum titer test was performed using an enzyme-linked immunosorbent assay (ELISA) by coating the antigen rhPD-L1 and following the manufacturer's instructions (Abcam, cat# ab214565). A high serum titer of a llama was achieved after four immunizations. Then, the peripheral blood of the llama was extracted, and lymphocytes were isolated using gradient centrifugation. Total RNA was isolated from lymphocytes with TRIzol Reagent (Invitrogen, cat# 15596018). The RNA template, via reverse transcription, produces complementary DNA (cDNA), which can be used directly as a template for polymerase chain reaction (PCR); the camelid VHH fragments were amplified using specific primers. Then, the camelid VHH fragments were ligated to the pMECS vector. Finally, a camelid VHH phage library was created by transforming the ligation products into XL1-Blue *E. coli* cells.

VHH phage display library amplification

To amplify the library, 200 μl of the PD-L1-VHH phage library was inoculated into 40 ml of superbroth medium [10 g of MOPS 3-(N-morpholino) propanesulfonic acid (Sigma, cat# 8899), 30 g of tryptone (BD-Bioscience, cat# 0123–17–3), and 20 g of yeast extract (BD-Bioscience, cat# 0127–17–9); 1 L ddH_2O)] containing 100 μg/ml ampicillin and 10 μg/ml tetracycline incubated at 37 °C and shaken at 220 rpm until an Optical Density (OD_{600}) of 0.8. Then, 10 μl (2.50×10^{11} colony-forming units (CFU)) of helper phage VCSM13 was added and incubated for 15 min at 37 °C without agitation. Then, the phage culture was incubated at 37 °C and shaken at 250 rpm for 2 h. After that, the bacteriophages were collected by spinning down at 4000 rpm/min for 10 min at room temperature. Then, the pellet was resuspended in 40 ml fresh superbroth medium containing 100 μg/ml ampicillin, 10 μg/ml tetracycline, and 50 μg/ml kanamycin. They were then incubated at 30 °C with agitation overnight. To transfer overnight culture to an autoclaved 50 ml centrifuge tube, the cells were centrifuged at 4000 rpm for 10 min at 4 °C. Next, the phages were precipitated from the bacteriophage supernatant using 5X polyethylene glycol (PEG)/sodium chloride (NaCl) (20% PEG/2.5 M NaCl). In addition, to resuspend the pellet with 1 ml of phosphate buffered saline (PBS). Repeat precipitated steps one more time to remove any bacterial cells. Finally, the phages were resuspended in 200 μl of PBS+1% bovine serum albumin (BSA) buffer.

VHH phage display library screening

To screen the PD-L1-specific VHH binders, as described previously [41]. Briefly, rhPD-L1-His-antigen was coated on the surface of a 96-well plate. Then, approximately 2.50×10^{11} CFU phages were added to the coated plates and incubated at 37 °C in a 220 rpm shaker for 15 min. To wash plates 6 times with 200 μl/well 0.1% phosphate-buffered saline with Tween 20 (PBST), the weakly bound or nonbinding phages were removed. To adjust the pH, the specific binders were eluted with 100 μl Glycine-BSA buffer ((0.2 M glycine-HCl, 1 mg/ml BSA, pH 2.2) and neutralized with 10 μl 2 M Tris base buffer (pH 9.0). These phage binders

are defined as output phages. The eluted phage-infected competent XL1 blue grew to mid-log phase with OD_{600}=0.6 and was amplified. This phage binder is defined as an input phage and used for the next panning rounds. The panning was repeated three times. After biopanning, we picked 86 clones and amplified them with VCSM13 helper phage in two 2 ml U-bottom 96-well deep blocks. A phage ELISA was performed using 100 μl of the phage supernatant per sample. The positive phage clones precipitated using PEG/NaCl and resuspended in 200 μl PBS. Quantification of bacteriophage by spectrophotometry.

ELISA

For the phage ELISA analysis, a 96-well ELISA plate (Thermo Scientific, Nunc) was coated with 100 μl/well of 2 μg/ml rhPD-L1 antigen in 0.1 M sodium bicarbonate (NaHCO3) (pH 8.6) buffer at 4 °C overnight. The plate was blocked with 200 μl 0.2% BSA blocking buffer and incubated at 37 °C for 2 h. Then, the plate was washed 2 times with 200 μl PBS containing 0.05% Tween-20 (pH 7.2). Add 50 μl of phage culture per well; duplicate wells are used for each clone, incubated at 37 °C for 1 h. The plate was washed 4 times with 200 μl PBS containing 0.05% Tween-20 (pH 7.2). Then, 50 μl of HRP/anti-M13 monoclonal conjugate (GE Healthcare Life Science, cat# 27–9420–01) diluted 1:5000 in PBS containing 1% BSA was added to each well and incubated at room temperature for 1 h. To wash the plate 4 times with 200 μl PBS containing 0.05% Tween-20 (pH 7.2), 50 μl per well of TMB substrate solution was added and incubated at 37 °C for 10~15 . Stop the reaction with 50 μl stopping buffer. Another uncoated rhPD-L1 antigen was used as a negative control and the same process as described above was performed. The absorbance of the plate was measured on a reader (Tecan) at 450 nm. The positive phage binders Optical Density (OD_{450}) =coated plate OD_{450}-uncoated plate OD_{450}. All of the experiments were repeated at least three times.

For PD-L1 ELISA analysis, recombinant human PD-L1 (Sino Biological, cat# 10084-H02H) or recombinant mouse PD-L1 (Sino Biological, cat# 50010-M02H) (0.1 μg/well) was coated at 4 °C overnight, and the plate was washed with 200 μl/well washing buffer once. Next, 200 μl/well blocking buffer (PBS+0.1% BSA) was added and incubated at 37 °C for 1 h to block nonspecific binding sites. Then, the plate was washed one time. Next, quantification of supernatants with unpurified anti-PD-L1 VHHs by using the BCA Protein Assay Kit (BioRad), then unpurified primary antibodies of anti-PD-L1 VHHs (10 μg/well, HEK-293F medium 100 μl/well) or different purified primary antibodies of PD-L1 and control antibody were added to each well of the plate and incubated at 37 °C for 1 h. Then, wash the plate five times. Next, the HRP anti-6X His-tag antibody (Abcam, cat# ab1187) or HRP-conjugated anti-human IgG (Fab')2 (Abcam, cat# ab87422) (1:2000) was added and incubated at 37 °C for 35 min. After washing five times, the substrate was added, and the absorbance of each well was read at 450 nm. All of the experiments were repeated at least three times.

Antibody design and purification

Diagrams of the anti-PD-L1 VHH single antibody are shown in Fig. 2A. Briefly, for anti-PD-L1 VHH, the single domain anti-PD-L1 VHH was fused with a His-tag. Anti-PD-L1-CD16a antibodies were constructed by fusing anti-PD-L1 and anti-CD16a single domain antibody (Gen Bank: ABQ52436.1) with a (GGGGS)3 linker (Fig. 3A, a). For anti-PD-L1-IL15, anti-PD-L1 VHH with IL15/IL15Ra and a (GGGGS)3 linker was used (Fig. 3A, b). The IL-15Ra sushi domain (GenBank: CAG33345.1, amino acid from 1 aa to 77 aa in UniProtKB) included the subsequent 12 amino acids from exon 3 as previously described [13]; IL15 (GenBank: CAA62616.1, amino acid from 30 aa to 162 aa in UniProtKB) and IL15/IL15Rα were linked with a SG2SG4SG3SG4SLQ peptide to mimic the physiological trans-presentation of IL-15 as previously described [13,42]. Finally, for anti-PD-L1-CD16a-IL15, anti--PD-L1-CD16a with IL15/IL15Ra with a (GGGGS)3 linker (Fig. 3A, c). Then, the fusion genes were cloned into the pcDNA3.1(+) vector with an IL-2 signal peptide, and a His-tag was added to the C-terminal end for protein detection and purification. The antibodies were finally expressed in HEK-293F cells, as previously described [14]. The fusion proteins were purified by a Ni-NTA affinity (QIAGEN, cat# 30210) purification system. After purification, samples of the antibodies were run on 10% sodium dodecyl sulfate–polyacrylamide gel electrophoresis (SDS–PAGE) gels under reducing conditions, and then the gel was stained with Coomassie brilliant blue R-250 dye (Thermo Fisher Scientific, cat# 20278). All of the experiments were repeated at least three times.

Flow cytometry analysis

For the flow cytometry analysis, LS174T and CHO cells were grown to 80%–90% confluence. First, the cells were digested with 0.25% trypsin, incubated at 37 °C, and collected. Then, 5×10^5 cells/sample were collected by centrifugation at 1000 rpm for 5 min. Then, the cells were washed with 1 ml of ice-cold phosphate-buffered solution (PBS)+ 0.2% bovine serum albumin (BSA) 2 times. The samples were then incubated with different antibodies (final concentration of 50 μg/ml) for 1 h on ice. The cells were then washed twice, and goat anti-human IgG ($H + L$) AF488 (Invitrogen, cat# A11013) or anti-6X His-tag FITC (Abcam, cat# ab1206) was used as the secondary antibody for another 1 h. After washing the cells three times, flow cytometry analysis was performed on an FC50 (FC 500, Beckman Coulter). All the experiments were repeated at least three times.

Affinity measurement

The affinity of anti-PDL1 antibodies to the extracellular part of the PD-L1 protein was determined using a ProteOn™ XPR36 Protein Interaction Array System (BIO-RAD). Briefly, human recombinant PD-L1 proteins with an Fc tag (Sino Biological, cat# 10084-H02H-B) in phosphate buffered saline with Tween 20 (PBST) were loaded onto the surface of a ProteOn XPR36 GLC chip. Immobilization levels between 1.0 and 1.5 nM were reached. The tested anti-PD-L1 antibodies were then applied in concentrations of 0 nM, 0.125 nM, 0.25 nM, 0.5 nM, 1 nM, and 2 nM. Then, the association and dissociation phases were measured for 200 s and 15 min, respectively. ProteOn data were analyzed by ProteOn Manager (version 2.0), and the relation between the association and dissociation is the equilibrium dissociation constant which equals the association rate constant divided by the dissociation rate constant (KD=Ka/Kd). All of the experiments were repeated at least three times.

Blood cell fractionation

Human peripheral blood mononuclear cells (PBMCs) were freshly prepared by Ficoll density centrifugation (GE Health) from blood that was collected from 11 health donors as described previously with some modifications [17,43]. According to the manufacturer's instructions, NK cells or T cells were then isolated from the PBMCs by EasySepTM Human NK Cell Enrichment Kit (Stem cell Co. Ltd, cat# 1905) or EasySepTM Human T Cell Enrichment Kit (Stem cell Co. Ltd, cat#19,661).

Cell proliferation analysis

For cell proliferation, CTLL-2 and T cells were harvested, washed twice with PBS, and incubated with RPMI 1640 with 10% FBS and 1% non-essential amino acid (NEAA) at 37 °C and 5% CO2. After 4 h of incubation, the cell suspension at a density of 2×10^4 cells/well was seeded into a 96-well plate with durvalumab (Creative Biolabs, cat# TAB-417CQ) or rhIL-15 or anti-PD-L1-VHH or anti-PD-L1-CD16a or anti-PD-L1-IL5 or anti-PD-L1-CD16a-IL15 at different concentrations (varied from 0.0001 to 1000 nM). After 72 h of incubation at 37 °C and 5% CO2, Cell Counting Kit-8 (Dojindo, cat# CK06–10) was performed. All of the

experiments were repeated at least three times.

CFSE labeling of T or NK cells and proliferation assay

To measure T cells or NK cells proliferation, T cells or NK cells were freshly prepared by Ficoll centrifugation, adjusted to 2×10^6 cells/ml, and then stained with 5 μM carboxyfluorescein succinimidyl ester (CFSE) (Biolegend, cat# 423801) according to the manufacturer's instructions. Stained T cells (0.5×10^6 cells/ml in 12-well plates) were incubated with 10 nM anti-PD-L1-IL5 or anti-PD-L1-CD16a-IL15 for 1 day. Stained NK cells (0.5×10^6 cells/ml in 12-well plates) were incubated with 10 nM durvalumab, rhIL-15, anti-PD-L1-VHH, anti-PD-L1-CD16a, anti-PD-L1-IL5 or anti-PD-L1-CD16a-IL15 for 5 days. Then, T cell (1 day) or NK cell (5 days) proliferation was assessed on an FC50 (FC 500, Beckman Coulter) and analyzed using FlowJo v10 software (BD-Biosciences).

Western-blot analysis

For western blotting were performed as described previously with some modifications [44–46], T cells were harvested, washed twice with PBS, and incubated with RPMI 1640 with 10% FBS and 1% NEAA at 37 °C, 5% CO2. After 4 h of incubation, the cells suspension at a density of 5×10^5 cells/well was seeded into the 96-wells plate with durvalumab or rhIL-15 or anti-PD-L1-VHH or anti-PD-L1-CD16a or anti-PD-L1-IL5 or anti-PD-L1-CD16a-IL15 at 100 nM. After 48 h of incubation at 37 °C, 5% CO2, cells were rinsed with ice-cold PBS twice and lysed with RIPA buffer (Sigma-Aldrich, cat#R0278) plus the protease inhibitor cocktail. Protein concentrations were determined using the BCA Protein Assay Kit (BioRad). About 25 μg protein per sample was loaded on a 10% SDS-PAGE gel and transferred to the polyvinylidene difluoride (PVDF) membrane, which was blocked with 5% milk in PBST, and incubated with the anti-STAT5 (Cell Signaling Technology, cat# 94205) or phospho-Stat5 (Tyr694) antibody (Cell Signaling Technology, cat# 9351) or GAPDH antibody (Cell Signaling Technology, cat# 2118) in the cold room overnight. After washing with PBST 3 times for 10 min each, the membranes were incubated with the horseradish peroxidase-conjugated secondary antibody (Abcam, cat# ab6721) at room temperature for one hour. The membranes were washed with PBST three times with 10 min and subjected to chemiluminescent western blot analysis. All of the experiments were repeated at least three times.

Cytotoxic assays

Cytotoxicity assays were performed as described previously with some modifications [16]. Briefly, CHO and LS174T cells were seeded into 96-well plates at a density of 2500 cells per well and incubated at 37 °C, 5% CO2 for 6 h. A total of 25,000 NK cells, T cells or NK+*T* mix cells and different concentrations of antibodies were added to each well. After 72 h incubation, removed the T cells and NK cells, then the CHO or LS174T cells viability was were measured by Cell Counting Kit-8 reagent (Dojindo) following the manufacturer's instruction. The OD at 450 nm was recorded by TECAN microplate reader. The survival rate (%) of CHO or LS174T cells was calculated using the following formula: [(live tumor cells (sample)-medium)/(live tumor cells (control)-medium)]. The NK or T cells insolate from 8 health donors. All of the experiments were repeated at least three times.

In vivo antitumour experiments

In vivo studies were performed as described previously [14,16]. Briefly, PD-L1-positive LS174T cells (1×10^6) were mixed with freshly isolated human PBMCs (5×10^6) (from two healthy donors). The mixed cells (200 μL/mouse) were then transplanted to the right flank of 5-week-old female nonobese diabetic/severe combined immunodeficiency (NOD/SCID) mice by subcutaneous injection. After transplantation for 1 h, durvalumab (3.5 mg/kg or 0.7 mg/kg), recombinant human Interleukin-15 (rhIL-15) (0.35 mg/kg or 0.07 mg/kg), anti-PD-L1-VHH (0.35 mg/kg or 0.07 mg/kg), anti-PD-L1-CD16a (0.7 mg/kg or 0.14 mg/kg), anti-PD-L1-IL15(0.9 mg/kg or 0.18 mg/kg), and anti-PD-L1-CD16a-IL15 antibodies (1.2 mg/kg or 0.24 mg/kg), and negative control (PBS) were administered intraperitoneally to 200 μL per mouse (i.p.) ($n = 6$ each group). Treatment was performed every two days. The volume of the tumor was measured every two days. tumor volume was calculated by the formula (width^2×length)/2.

To further validate the antitumor activities of anti-PD-L1 antibodies *in vivo*. 1×10^6 LS174T cells with 200 μL PBS per mouse, the cell suspensions were then injected subcutaneously into the right flank of NOD scid gamma mouse (NSG) mice (female, 6 weeks old). Then, PBMCs freshly were isolated from 1 healthy donor, and different anti-PD-L1 antibodies or PBS were administered intraperitoneally when the tumor size reached 50–100 mm^3. Anti-PD-L1 antibodies or rhIL-15 treatment was performed every two days. In addition, mice were weighed, and tumor growth size was recorded every two days. tumor volume was calculated by the formula (width^2×length)/2. All animal experiments were carried out with the approval of the Ethics Committee of Guangxi Medical University and were performed in accordance with the Institutional Animal Welfare Guidelines set by Guangxi Medical University.

Results

Phage display library construction and single-domain antibody screening

We constructed a library of anti-PD-L1 single domain antibodies. First, llamas were immunized seven times with 300 μg of PD-L1 recombinant human protein. Then, we isolated lymphocytes from the llamas immunized and constructed a phage library. Next, we conducted three rounds of panning on phage, and anti-PD-L1 phages were significantly enriched (Table 1). After panning, we randomly picked 86 clones and expanded them by incubating them overnight at 37 °C and 220 rpm. After that, we performed an ELISA using 100 μl phage medium per sample. The results showed that 31 out of 86 clones recognized the rhPD-L1 antigen (data not shown). In addition, 31 positive phage clone supernatants with PEG/NaCl solution are an easy way to obtain higher viral titers by concentrating virus. Finally, the pellet was resuspended in 200 μl PBS. The phage concentration measured the OD value of A280. Furthermore, the quantitative ELISA analysis was performed. The positive phage binders OD_{450}=coated plate OD_{450}-uncoated plate OD_{450}. The data showed that 16 positive clones specifically recognized the rhPD-L1-His-antigen (Figs. 1 and S1).

The anti-PD-L1-VHH single domain antibody can be produced and purified in HEK-293F cells

The anti-PD-L1-VHH antibody was constructed by fusing two parts:

Table 1
Enrichment data for the PD-L1-VHH library.

	1st Round 1 μg rhPD-L1	2nd Round 500 ng rhPD-L1	3rd Round 200 ng rhPD-L1
Input phage (cfu)	2.50×10^{11}	2.50×10^{12}	5.00×10^{12}
Output phage (cfu)	3.50×10^{6}	5.50×10^{8}	4.00×10^{10}
Output/Input	1.40×10^{-5}	2.20×10^{-4}	8.00×10^{-3}

rhPD-L1 antigen (1 μg) was coated in a 96-well plate. Then, the phage library containing approximately 2.50×10^{11} cfu phages was input. The input phages were incubated with the coated plates for 15 min at 37 °C. The weakly bound phages or nonspecific phage binders were washed away. Specific binder phages were eluted and named the Output. The eluted phage binders were used to infect competent *E. coli* XL1-blue and amplified for the next rounds. To enrich the positive binders, the panning was performed for 3 rounds by coating decreased rhPD-L1 antigen from 1 μg to 200 ng in each cycle, which increased stringency.

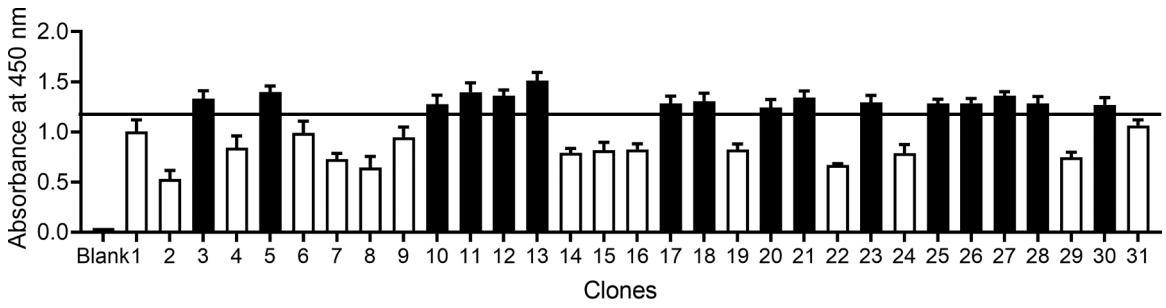

Fig. 1. Anti-hPD-L1 single domain antibody screening
ELISA was performed using 1 μg of purified and quantified phage to pick up 16 positive clones (OD 450 ≥ 1.20, black bars). The positive phages binders OD_{450}=coated plate OD_{450}-uncoated plate OD_{450}. The results are the averages of duplicates from three independent experiments. Data are the means ± SEM. See also Fig. S1.

anti-PD-L1 single-domain antibodies targeting PD-L1-overexpressing cancer cells. In addition, a His-tag was added at the C-terminus to facilitate protein purification and detection (Fig. 2A). To further analyze the positive clones, an ELISA was performed to investigate the binding of the anti-PD-L1-VHH antibody to the rhPD-L1 antigen. The anti-PD-L1-VHH antibody can be produced in HEK-293F cells. On posttransfection day 6, we collected the supernatant. Again, an ELISA was performed, and the data showed that clone #13 showed a large obvious difference in binding to the rhPD-L1 antigen compared with other clones (Fig. 2B). Based on the results, clone #13 was further analysed.

The anti-PD-L1-VHH single domain antibody can bind PD-L1-overexpressing tumor cells

To study the function of the anti-PD-L1-VHH antibody, clone #13 antibody was expressed in HEK-293F cells. The clone #13 antibody was soluble and purified by Ni-NTA affinity chromatography purification, and the anti-PD-L1-VHH antibody with molecular weights of ~15 kDa was obtained (Fig. 2C).

Furthermore, ELISA was performed to check the binding of the anti-PD-L1-VHH antibody to the rhPD-L1 antigen. Both anti-PD-L1-VHH antibody and durvalumab could bind to rhPD-L1 protein (Fig. 2D). Therefore, these results suggested that the anti-PD-L1-VHH antibody has a strong binding affinity for the rhPD-L1 protein.

In addition, to check whether the anti-PD-L1-VHH antibody can bind to PD-L1-overexpressing tumor cells, flow cytometry analysis was performed using PD-L1-positive cancer cells, LS174T cells, PD-L1-negative CHO cells. For PD-L1-positive cancer cells, LS174T, anti-PD-L1-VHH, or positive antibody (durvalumab) showed positive staining (Fig. 2E, right panel) but very low or no staining on the PD-L1-negative cell line CHO (Fig. 2E, left panel), suggesting that the anti-PD-L1-VHH antibody binds specifically to PD-L1-positive tumor cells. To further evaluate the binding of anti-PD-L1 antibodies to PD-L1, the affinity of anti-PD-L1 VHH to PD-L1 was measured. The data showed that anti-PD-L1-VHH have affinity of 1.04–09 M. In addition, the affinities of the previously mentioned antibodies (1.0–09 M) indicates good candidates for further study [47], suggesting that anti-PD-L1-VHH have good affinity.

To test whether anti-PD-L1-VHH cross-reacts with murine PD-L1, ELISA was performed. The results showed that neither durvalumab nor anti-PD-L1-VHH were cross-reactive with murine PD-L1 (Fig. 2F). Furthermore, ELISA competition assays were performed to examine whether durvalumab and anti-PD-L1-VHH bound to the same epitope. The results showed that both durvalumab and anti-PD-L1-VHH can recognize the rhPD-L1 protein. However, the effect of anti-PD-L1-VHH on rhPD-L1 protein was not abolished by durvalumab. These data showed that neither durvalumab nor anti-PD-L1-VHH bound to the same epitope (Fig. 2G).

Anti-PD-L1-CD16a-IL15 stimulates immune cell proliferation in vitro

Anti-PD-L1-CD16a-IL15 was constructed to contain three functional modules (Fig. 3A). The anti-PD-L1 VHH targets PD-L1-overexpressing tumor cells; anti-CD16a VHH engage NK cells; and the IL-15/IL-15Ra complex activates and increases in the NK cells and T cells population. In addition, a histidine tag was added to the carboxyl terminus for detection and purification. The fusion gene of anti-PD-L1-CD16a-IL15 was cloned into the pcDNA3.1(+) vector and then transiently transfected into HEK-293F cells. Anti-PD-L1-CD16a as a control antibody was constructed to contain anti-PD-L1-VHH, anti-CD16a VHH, and His-tag. Anti-PD-L1-IL15, another control antibody, contained anti-PD-L1-VHH and IL-15/IL-15Ra complexes and His-tag. These fusion proteins were purified from the HEK-293F cell culture medium by Ni-NTA affinity chromatography. Bands of ~28 kDa (anti-PD-L1-CD16a), 38 kDa (anti-PD-L1-IL15), and 53 kDa (anti-PD-L1-CD16a-IL15) were observed under reducing conditions (Fig. 3B).

The cytokine activity of anti-PD-L1-CD16a, anti-PD-L1-IL15, and anti-PD-L1-CD16a-IL15 was then assessed using a cytokine-dependent cell proliferation assay with the CTLL-2 cell line and human T cells. The purpose is to assess IL-15/IL-15Ra complex activity. The data showed that all the rhIL-15, anti-PD-L1-IL15 and anti-PD-L1-CD16a-IL15 dramatically stimulated the proliferation of the CTLL-2 cell line and human T cells at a similar level, not anti-PD-L1-VHH, anti-PD-L1-CD16a and durvalumab, demonstrating that the IL-15/IL-15Ra complex of anti-PD-L1-IL15 and anti-PD-L1-CD16a-IL15 maintains IL-15 cytokine activity (Fig. 3C).

To measure the activity of anti-PD-L1-CD16a, anti-PD-L1-IL15, and anti-PD-L1-CD16a-IL15 on primary immune cells, human T cells or NK cells were prepared, T cells stained with CFSE and incubated with anti-PD-L1-IL15, and anti-PD-L1-CD16a-IL15 for 1 day and NK cells stained with CFSE and incubated with durvalumab, rhIL-15, anti-PD-L1-VHH, anti-PD-L1-CD16a, anti-PD-L1-IL15, and anti-PD-L1-CD16a-IL15 for 5 days. After 1 day, anti-PD-L1-IL15 and anti-PD-L1-CD16a-IL15 significantly stimulated proliferation in human T cells compared to cells in the control group (Fig. 3D). After 5 days, rhIL-15, anti-PD-L1-IL15 and anti-PD-L1-CD16a-IL15 significantly stimulated the proliferation of human NK cells, and anti-PD-L1-CD16a and durvalumab but not anti-PD-L1-VHH slightly stimulated the proliferation of human NK cells (Fig. 3E).

The effects of anti-PD-L1-CD16a-IL15 treatment on the activation of STAT-signaling pathways were then evaluated using human T cells. Following receptor engagement, IL-15 signaling activates signal transducer and activator of transcription 5 (STAT5) transcription factors, to exert its regulatory functions in immune cells [48]. Indeed, in human T cells, compared to vehicle, rhIL-15 or anti-PD-L1-IL15 or anti-PD-L1-CD16a-IL15 induced an increase in STAT5 phosphorylation (Fig. 3F). Different from anti-PD-L1-CD16a-IL15, both anti-PD-L1-VHH and anti-PD-L1-CD16a showed no effects on the phosphorylation of STAT5 in T cells (Fig. 3F). These results suggest that

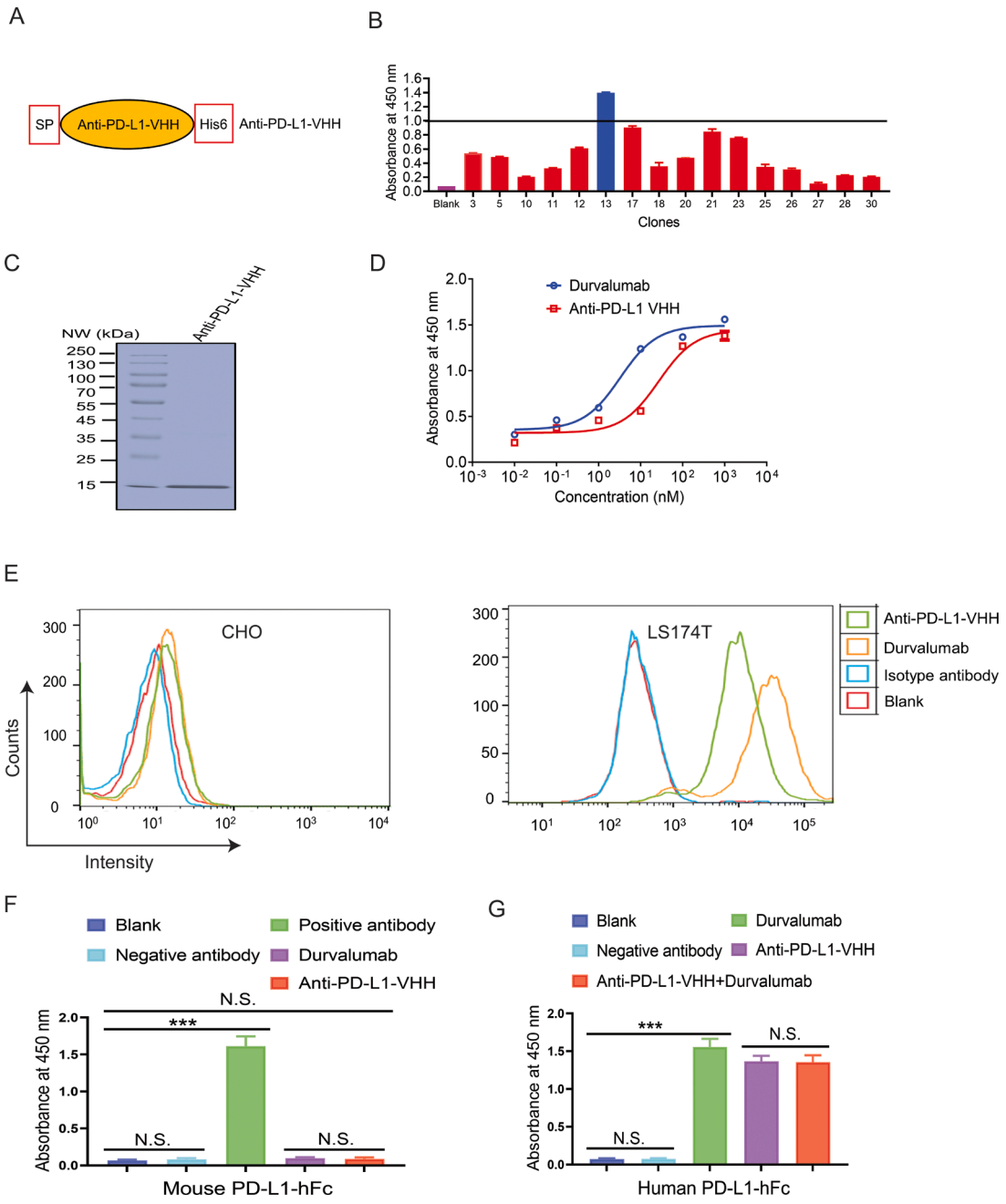

Fig. 2. Biochemical characterization of anti-PD-L1 VHH

(A) Schematic representation of anti-PD-L1 VHH consisting of IL-2 signal peptide, anti-PD-L1 single domain antibody, and His-tag. (B) ELISA analysis of an anti-PD-L1-positive single domain antibody. On day 6 posttransfection, 10 μg/sample of HEK-293F culture supernatant was collected for ELISA to identify positive clone #13 (OD $_{450} \geq 1$). (C) Coomassie blue staining of anti-PD-L1 VHH, approximately 15 kDa. (D) ELISA detected anti-PD-L1-VHH and anti-PD-L1 positive antibodies (durvalumab) as controls. (E) Flow cytometry analysis of anti-PD-L1-VHH and duvalumab using LS174T cells as positive and CHO cells as negative cells. (F) ELISA analysis of different antibodies: negative antibody (human IgG isotype control, Invitrogen, cat #02–7102), positive antibody (goat anti-mouse PD-L1 antibody, R&D systems, cat# AF1019), durvalumab (Creative Biolabs, cat# TAB-417CQ), and anti-PD-L1-VHH using as primary antibodies, and recombinant mouse PD-L1 as coated antigen. (G) ELISA analysis of different antibodies: negative antibody, positive antibody, duvalumab, and anti-PD-L1-VHH using as primary antibodies, and recombinant human PD-L1 as coated antigen. The results are the averages of duplicates from three independent experiments. Data are the means ± SEM, N.S., not significant, $^{**}P < 0.01$; $^{**}P < 0.001$ compared with the control.

anti-PD-L1-CD16a-IL15 have significant effects on the STAT5-signaling pathway.

Anti-PD-L1-CD16a-IL15 mediates potent cytotoxic activities against PD-L1-positive tumor cells

To check whether anti-PD-L1-CD16a, anti-PD-L1-IL15, and anti-PD-L1-CD16a-IL15 can mediate specific tumor cell killing, cytotoxic assays were performed using the PD-L1-positive cell lines LS174T and the PD-L1-negative cell line CHO. Both LS174T and CHO cell lines were incubated with durvalumab, rhIL-15, anti-PD-L1-VHH, anti-PD-L1-CD16a, anti-PD-L1-IL15, and anti-PD-L1-CD16a-IL15 in the presence of T cells, NK cells, or mixed T cells and NK cells, respectively (Figs. 4 and S2). For PD-L1-negative CHO cells, durvalumab, rhIL-15, anti-PD-L1-VHH, anti-PD-L1-CD16a, anti-PD-L1-IL15, and anti-PD-L1-CD16a-IL15 had no cell killing activity either alone or in the presence of NK

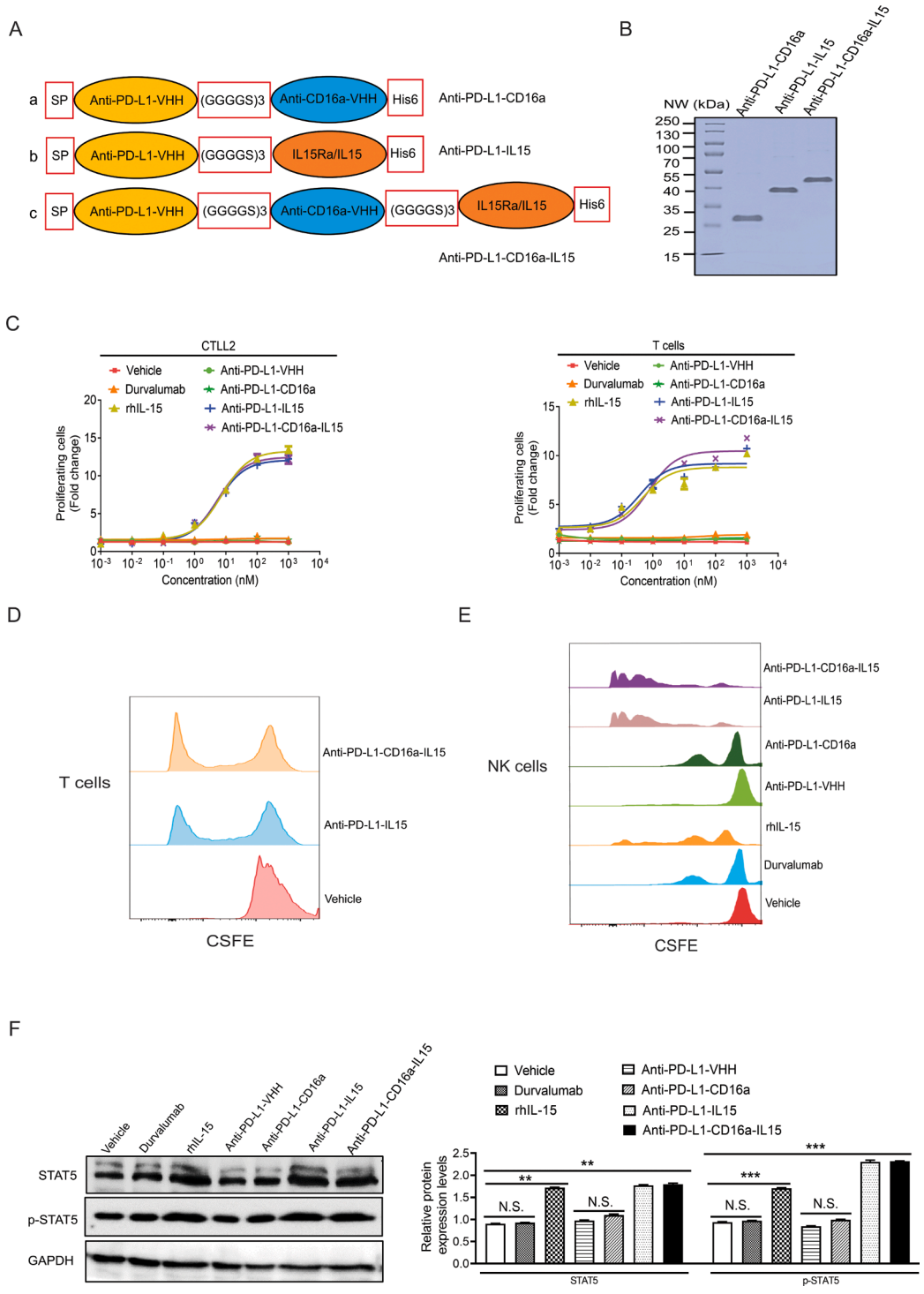

Fig. 3. Biochemical characterization of the anti-PD-L1-CD16a-IL15 fusion protein

(A) Schematic representation of anti-PD-L1-CD16a and anti-PD-L1-IL15 and anti-PD-L1-CD16a-IL15 fusion proteins. (B) Coomassie blue staining of anti-PD-L1-CD16a (28 kDa), anti-PD-L1-IL15 (38 kDa), and anti-PD-L1-CD16a-IL15 (53 kDa) fusion proteins.

(C) In the left panel, CTLL-2 proliferation stimulated by durvalumab, rhIL-15, anti-PD-L1-VHH, anti-PD-L1-CD16a and anti-PD-L1-IL15, and anti-PD-L1-CD16a-IL15. In right panel, human T cell proliferation was stimulated by durvalumab, rhIL-15, anti-PD-L1-VHH, anti-PD-L1-CD16a and anti-PD-L1-IL15, and anti-PD-L1-CD16a-IL15.(D) T-cell proliferation stimulation *in vitro* by anti-PD-L1-IL15, and anti-PD-L1-CD16a-IL15. CFSE-labeled T cells were incubated with 10 nM of different proteins for 1 day. The proliferation of T cells was assessed by flow cytometry.(E) NK-cell proliferation stimulation *in vitro* by durvalumab, rhIL-15, anti-PD-L1-VHH, anti-PD-L1-CD16a, anti-PD-L1-IL15, and anti-PD-L1-CD16a-IL15. CFSE-labeled NK cells were incubated with 10 nM of different proteins for 5 days. The proliferation of NK cells was assessed by flow cytometry. (F) Human T cell proliferation was stimulated by durvalumab, rhIL-15, anti-PD-L1-VHH, anti-PD-L1-CD16a and anti-PD-L1-IL15, and anti-PD-L1-CD16a-IL15, then total cell lysates were analyzed by immunoblot for the STAT5 protein or STAT5 phosphorylated protein or GAPDH protein. The protein expression level, quantified by band intensity and normalized to GAPDH, is displayed in the right panel. The results are the averages of duplicates from three independent experiments. Data are the means ± SEM, N.S., not significant, $^{**}P < 0.01$; $^{**}P < 0.001$ compared with the control.

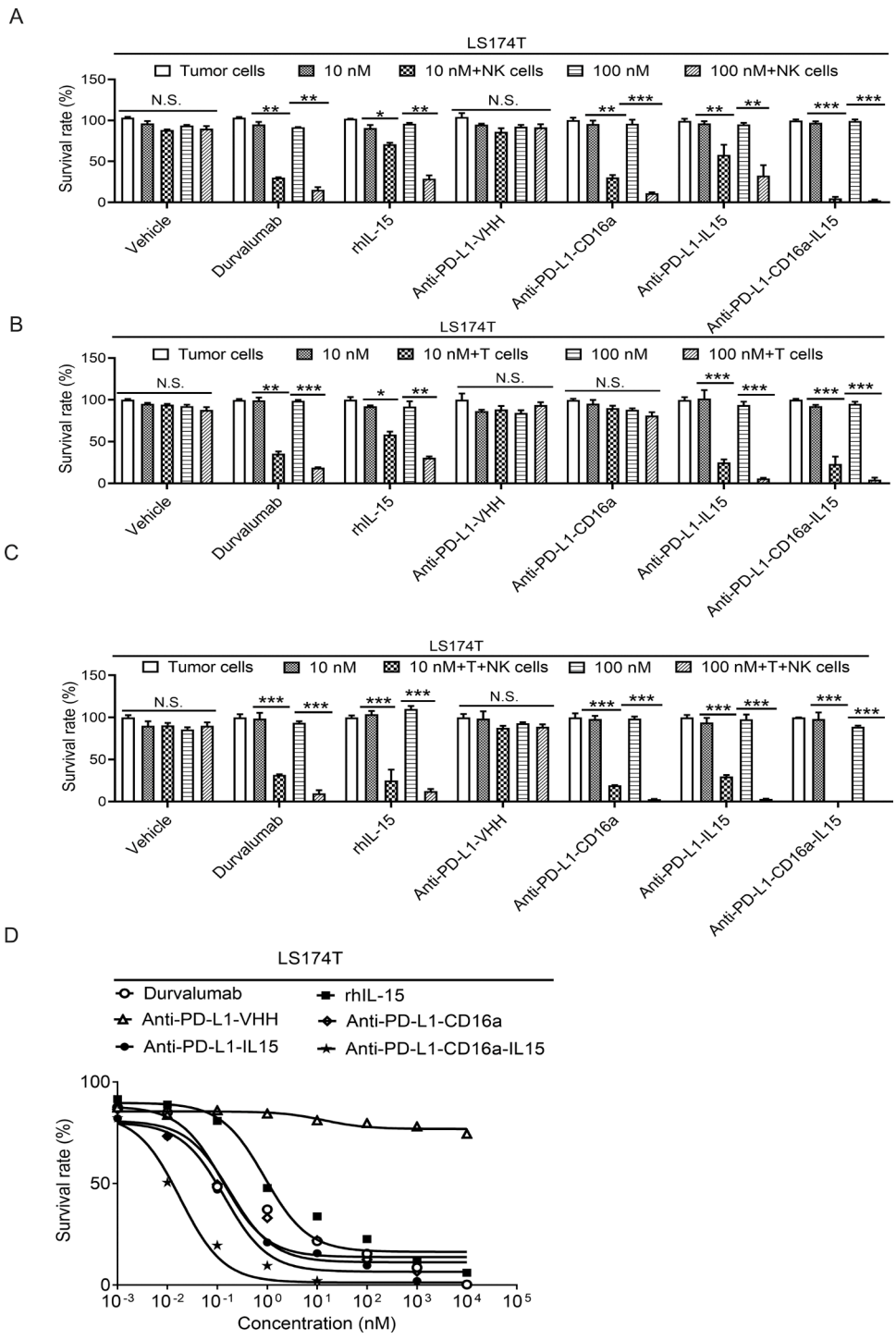

Fig. 4. Anti-PD-L1-CD16a-IL15 fusion protein induces NK or T cell-mediated cytotoxicity
(A) Different cell lines were treated with durvalumab, rhIL-15, anti-PD-L1-VHH, anti-PD-L1-CD16a, anti-PD-L1-IL15 or anti-PD-L1-CD16a-IL15 antibodies and freshly isolated NK cells. The effector (NK cells) (25,000 cells/well) and target LS174T cells (2500 cells/well) at a ratio of 10:1. (B) Different cell lines were treated with durvalumab, rhIL-15, anti-PD-L1-VHH, anti-PD-L1-CD16a, anti-PD-L1-IL15, or anti-PD-L1-CD16a-IL15 with freshly isolated T cells. The effector (T cells) (25,000 cells/well) and target LS174T cells (2500 cells/well) at a ratio of 10:1. (C) Different cell lines were treated with durvalumab, rhIL-15, anti-PD-L1-VHH, anti-PD-L1-CD16a, anti-PD-L1-IL15, or anti-PD-L1-CD16a-IL15 with freshly isolated *T*+NK cells. The effector (T:NK cells at a ratio of 1:1) (25,000 cells/well) and target LS174T cells (2500 cells/well) at a ratio of 10:1. (D) Different cell lines were treated with durvalumab, rhIL-15, anti-PD-L1-VHH, anti-PD-L1-CD16a, anti-PD-L1-IL15, or anti-PD-L1-CD16a-IL15 fusion proteins with freshly isolated *T*+NK cells. The effector (T:NK cells at a ratio of 1:1) (25,000 cells/well) and target LS174T cells (2500 cells/well) at a ratio of 10:1. All fusion proteins induce *T*+NK cell-mediated cytotoxicity in a dose-dependent manner. The results are the averages of duplicates from three independent experiments. Data are the means ± SEM, N.S., not significant, $*P < 0.05$; $**P < 0.01$; $** P < 0.001$ compared with the control.
See also Fig. S2.

cells (Fig. S2A), T cells (Fig. S2B), or mixed NK cells and T cells (Fig. S2C). For PD-L1-positive tumor cells, LS174T, durvalumab, rhIL-15, anti-PD-L1-VHH, anti-PD-L1-CD16a, anti-PD-L1-IL15, and anti-PD-L1-CD16a-IL15 alone had no cell killing activity at 10 nM or 100 nM (Fig. 4A and 4B and 4C). However, potent cell killing was observed in the presence of NK cells (Fig. 4A), T cells (Fig. 4B) or NK+ T cells (Fig. 4C). In addition, higher cell killing was observed when NK or T or NK+*T* (NK:*T* = 1:1) cells to the tumor cells ratio was 10:1 for both lower concentration 10 nM and higher concentration 100 nM anti-PD-L1-CD16a-IL15. First, in the presence of NK cells, all the durvalumab, rhIL-15, anti-PD-L1-CD16a, anti-PD-L1-IL15, and anti-PD-L1-CD16a-IL15 antibodies had cell killing activity against the PD-L1-positive tumor cell line LS174T. Furthermore, anti-PD-L1-CD16a-IL15 showed much stronger cell killing activity than all of them (Fig. 4A). Second, in the presence of T cells, all the durvalumab, rhIL-15, anti-PD-L1-IL15, and anti-PD-L1-CD16a-IL15 antibodies have potent cell killing activities against LS174T. However, anti-PD-L1-CD16a showed no cell killing, which may be because CD16a cannot activate T cells (Fig. 4B). Third, in the presence of NK and T cells, all the durvalumab, rhIL-15, anti-PD-L1-CD16a, anti-PD-L1-IL15, and anti-PD-L1-CD16a-IL15 antibodies have potent cell killing activities against LS174T. Anti-PD-L1-CD16a-IL15 showed much stronger cell killing activity than other antibodies (Fig. 4C).

Dose-dependent cell killing by anti-PD-L1-CD16a, anti-PD-L1-IL15,

and anti-PD-L1-CD16a-IL15 was further analysed using different concentrations of anti-PD-L1-CD16a, anti-PD-L1-IL15, and anti-PD-L1-CD16a-IL15. No cytotoxic activity against CHO cells was observed regardless of the presence of NK+T cells or the concentrations of anti-PD-L1-CD16a, anti-PD-L1-IL15, and anti-PD-L1-CD16a-IL15 (Fig. S2D). However, for PD-L1-positive cells, LS174T (Fig. 4D), increased cytotoxic activities were observed with increased concentrations of anti-PD-L1-CD16a, anti-PD-L1-IL15, and anti-PD-L1-CD16a-IL15 in the presence of NK+ T cells. Interestingly, anti-PD-L1-CD16a-IL15 shows much stronger activities than anti-PD-L1-CD16a and anti-PD-L1-IL15. These data suggested that the cytotoxic activity of anti-PD-L1-CD16a, anti-PD-L1-IL15, and anti-PD-L1-CD16a-IL15 depends on the expression of PD-L1 and the presence of NK+ T cells. In addition, the anti-PD-L1-CD16a-IL15 fusion protein is considered a novel therapy for cancer.

Anti-PD-L1-CD16a-IL15 targets tumor tissues and has potent antitumour activities in vivo

To evaluate whether anti-PD-L1-CD16a, anti-PD-L1-IL15, and anti-PD-L1-CD16a-IL15 can suppress tumor growth *in vivo*. First, LS174T PD-L1-positive cancer cells were grafted into NOD/SCID mice. Then, LS174T cells were transplanted together with freshly prepared human PBMCs into NOD/SCID mice. When mice were treated with durvalumab, rhIL-15, anti-PD-L1-VHH, anti-PD-L1-CD16a, anti-PD-L1-IL15, and anti-PD-L1-CD16a-IL15 in the presence of PBMCs, dramatic tumor growth inhibition was observed (Fig. 5A). However, anti-PD-L1-CD16a-IL15

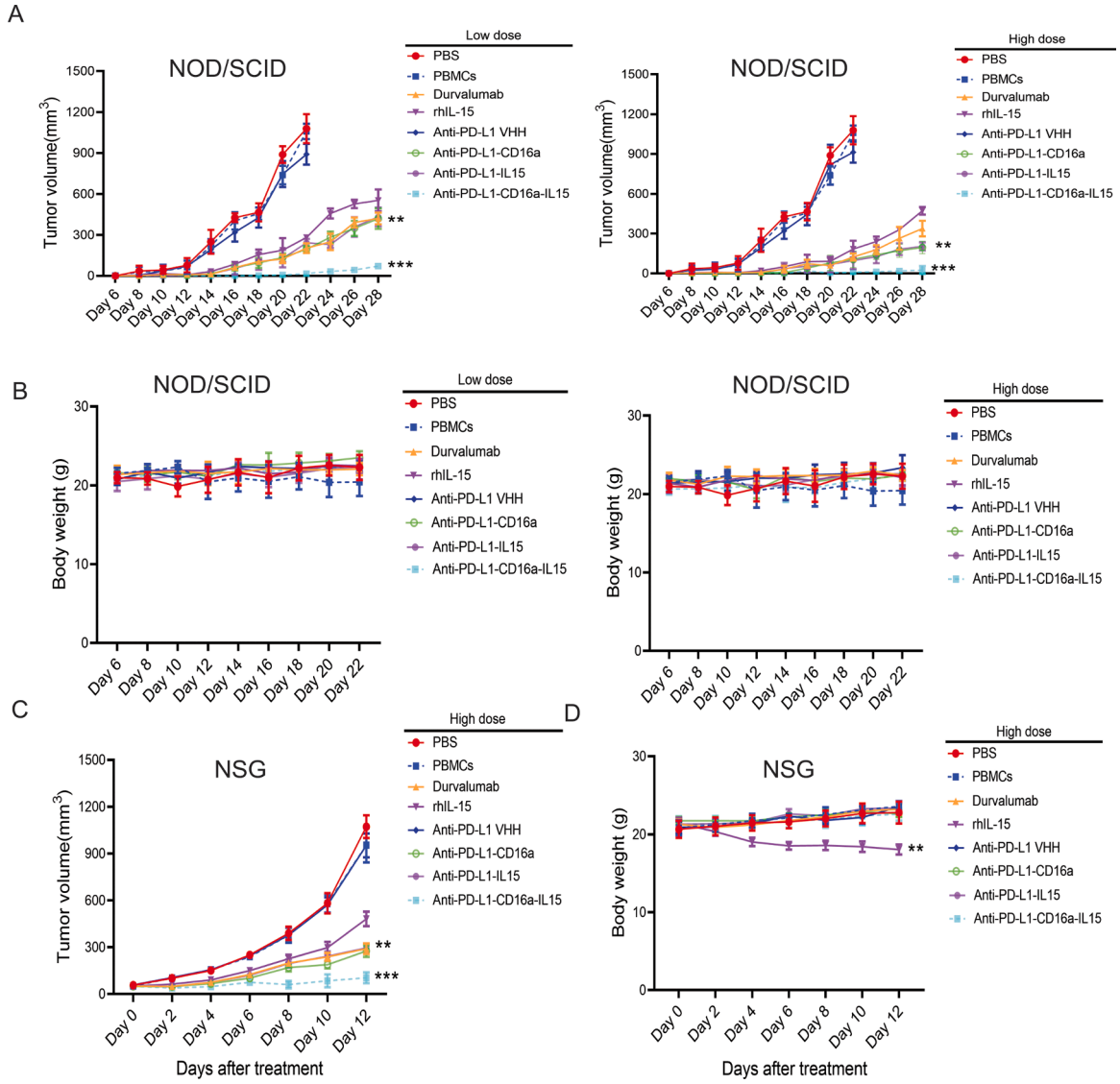

Fig. 5. Anti-PD-L1-CD16a-IL15 fusion protein inhibits tumor growth *in vivo*
(A) NOD/SCID mice, female, 4~5 weeks old, (weight 18–22 g) ($n = 6$ per group). All mice were subjected to subcutaneous injection (s.c.) with a prepared 0.2 mL mixture of LS174T cells (1×10^6/mouse) and PBMCs (5×10^6/mouse). Mice were then administered PBS or durvalumab (high dose: 3.5 mg/kg or low dose: 0.7 mg/kg), rhIL-15 (high dose: 0.35 mg/kg or low dose: 0.07 mg/kg), anti-PD-L1-VHH (high dose: 0.35 mg/kg or low dose: 0.07 mg/kg), anti-PD-L1-CD16a (high dose: 0.7 mg/kg or low dose: 0.14 mg/kg), anti-PD-L1-IL15(high dose: 0.9 mg/kg or low dose: 0.18 mg/kg), and anti-PD-L1-CD16a-IL15 antibodies (high dose: 1.2 mg/kg or low dose: 0.24 mg/kg) intraperitoneally every two days. tumor volumes of different treatment groups were measured. (B) The body weight of animals in different treatment groups during administration. (C) NSG mice, female, 6 weeks old ($n = 6$ per group). All mice were subjected to subcutaneous injection (s.c.) with a prepared 0.2 mL of LS174T cells (1×10^6/mouse). When the tumor volume reached 50–100 mm^3. Mice were then administered PBS or durvalumab (3.5 mg/kg), rhIL-15 (0.35 mg/kg), anti-PD-L1-VHH (0.35 mg/kg), anti-PD-L1-CD16a (0.7 mg/kg), anti-PD-L1-IL15 (0.9 mg/kg), and anti-PD-L1-CD16a-IL15 (1.2 mg/kg) intraperitoneally every two days. tumor volumes of different treatment groups were measured. (D) The body weight of mice in different treatment groups during administration. Data are the means ± SEM, N.S., not significant, $^{**}P < 0.01$; $^{**}P < 0.001$ compared with the control.

shows stronger antitumour activities than all the durvalumab, rhIL-15, anti-PD-L1-CD16a, anti-PD-L1-IL15. For the mice treated with PBS alone, no significant tumor growth inhibition was observed. Furthermore, the mice were also treated with the same molar amount of the control antibody anti-PD-L1 VHH, which recognizes PD-L1-positive cells in the presence of PBMCs. As anti-PD-L1 VHH cannot activate immune cells, no significant tumor growth inhibition was observed for anti-PD-L1 VHH treatment (Fig. 5A). In addition, no weight loss or apparent toxicity was observed in any mouse (Fig. 5B). These data confirmed that anti-PD-L1-CD16a-IL15 can inhibit PD-L1-positive tumor growth *in vivo*.

To further evaluate anti-PD-L1-CD16a-IL15 antitumor activity, a synergic model using the NSG mice was also evaluated. After transplanting LS174T cells in NSG mice, rapid tumor growth was observed. When the tumor volume reached 50 to 100 mm^3, the mice were administered freshly isolated human PBMCs and treated with PBS, durvalumab, rhIL-15, anti-PD-L1-CD16a, anti-PD-L1-IL15, and anti-PD-L1-CD16a-IL15 every 2 days. Tumor growth inhibition was then measured (Fig. 5C). Interestingly, anti-PD-L1-CD16a-IL15 showed stronger antitumor effects than durvalumab, rhIL-15, anti-PD-L1-CD16a, and anti-PD-L1-IL15. However, rhIL-15 treatment resulted in severe systemic toxicity, as indicated by dramatic body weight loss, which was consistent with previous report [49] (Fig. 5D). Interestingly, no weight loss or apparent toxicity was observed in any other group (Fig. 5D). We hypothesize that anti-PD-L1 fusion proteins improve tumor tissue penetration, reduce the off-tumor expansion of NK cells or T cells, diminish systemic toxicity, and efficiently inhibit tumor growth. These data demonstrated that anti-PD-L1-CD16a-IL15 has potent *in vivo* antitumor effects without gross toxicity in NSG mice.

Discussion

Programmed death-ligand 1 (PD-L1) is also known as cluster of differentiation 274 (CD274) or B7 homologue 1 (B7-H1) [50]. When PD-L1 binds to its receptor, PD-1, the PD-1 signal activates T cells, B cells, and myeloid cells to modulate strong activation or inhibition [51]. There is also emerging evidence that PD-L1 recognizes its receptor PD-1 on T cells to deliver a signal that suppresses TCR-mediated activation of IL-2 and T cell proliferation [52]. However, it appears that overexpression of PD-L1 may help cancers escape host immune responses [21,50]. Thus, PD-L1 is a cancer immunotherapy target, as it is upregulated in various cancers, including non-small-cell lung cancer (NSCLC) [53], anal carcinoma [54], cervical carcinoma [55], head and neck cancers [56], and hepatocellular carcinoma (HCC) [57]. This study screened anti-PD-L1 VHH single-domain antibodies from the phage display library and purified anti-PD-L1-VHH antibodies from HEK-293F cells. In addition, we tested the anti-PD-L1 antibodies function in PD-L1-overexpressing cancer *in vitro* and *in vivo*. In summary, our study confirmed that anti-PD-L1-CD16a and anti-PD-L1-IL15 and anti-PD-L1-CD16a-IL15 fusion proteins have potent antitumour activity against PD-L1-positive cancer cells.

IL-15 is a potential immunotherapy candidate for cancer, and it can stimulate the proliferation of T cells and NK cells [6]. However, the defect in IL-15 is its nonspecific systemic distribution, which leads to toxicity in various tissues [10]. Thus, their efficacy as immunity therapy is limited. To reduce the toxicity of IL-15, researchers selectively localized IL-15 in the tumor to minimize toxicity. Therefore, a tumor microenvironment that uses RGD peptides to target IL-15 was constructed, and it has been previously shown to have strong antitumor activity [13]. In addition, anti-CEA-IL15 induced strong immune cell proliferation and antitumor activity *in vitro* and *in vivo* [14]. In this study, to increase the local concentration of IL-15 in tumor tissues, anti-PD-L1 VHH was fused with anti-CD16a VHH and IL-15/IL-15Ra (Fig. 3A). First, anti-PD-L1 VHH showed a strong binding affinity, enhanced tumor targeting and reduced toxicity. In addition, IL-15/IL-15Ra could amplify T cells and NK cells, and the anti-CD16a VHH antibody could engage NK cells to enhance their ability to kill tumor cells. Furthermore, the use of anti-PD-L1-CD16a-IL15 (53 kDa) instead of regular IgG (150 kDa) reduced the molecular weight of anti-PD-L1-CD16a-IL15 by approximately 3 times, which may improve tumor tissue penetration. Interestingly, the function of anti-PD-L1-CD16a-IL15 is similar to that of anti-PD-L1 bispecific antibodies. However, compared to those of mAbs, the lower molecular weights of anti-PD-L1-CD16a, anti-PD-L1-IL15 and anti-PD-L1-CD16a-IL15 may have the disadvantage of more rapid clearance *in vivo*. To enhance its potential in the clinic, conjugation of anti-PD-L1-CD16a-IL15 with PEG or other means to increase the *in vivo* half-life may be considered.

The ELISA results suggested that anti-PD-L1-VHH did not share the same binding epitope as durvalumab on the rhPD-L1 protein (Fig. 2G). This provides great potential for using anti-PD-L1-CD16a-IL15, alone or in combination with durvalumab, to treat PD-L1-positive cancer. The combination therapy of trastuzumab with pertuzumab, another anti-Her2 antibody that binds to a different epitope than trastuzumab, is more effective in the clinic [58,59]. In addition, we are assessing whether anti-PD-L1-CD16a-IL15 has synergistic effects in inhibiting PD-L1-positive tumors when in combination with durvalumab, avelumab, or atezolizumab. This study will provide potentially more effective combinations than the current treatments in PD-L1-positive cancer.

In summary, we provide a novel format for a trifunctional antibody-fusion protein, anti-PD-L1 VHH, with anti-CD16a VHH and IL-15/IL-15Ra. This format consisted of a tumor-directed anti-PD-L1 single domain antibody, anti-CD16a VHH, and IL-15/IL-15Ra. In addition, anti-PD-L1-CD16a-IL15 fusion proteins can be expressed and purified from HEK-293F cells with good solubility and stability. Furthermore, the flow cytometry assay and ELISA showed that the anti-PD-L1 VHH antibody could bind to PD-L1-positive cells. Interestingly, anti-PD-L1-CD16a-IL15 fusion proteins also potently and specifically stimulate immune cell proliferation *in vitro*. *In vivo* studies demonstrated that anti-PD-L1-CD16a-IL15 fusion proteins could suppress tumor growth in the presence of PBMCs in NOD/SCID and NSG mice.

In conclusion, considering its potential anticancer activities, the lower molecular weight of anti-PD-L1-CD16a-IL15 may allow for improved tumor tissue penetration, reduce the off-tumor expansion of NK cells or T cells, diminish systemic toxicity, and efficiently inhibit tumor growth. The potential to use anti-PD-L1-CD16a-IL15 to treat PD-L1-overexpressing cancer combined with current anti-PD-L1 therapeutics. Therefore, trifunctional antibody-fusion proteins provide a new promising immunity therapeutic.

Author contributions

Conception and design of the study: Y.L., X.F., H.W.; experimental performance: Y.L., L.W., Y.L., S.M., B.H; data collection and analysis and explanation of experiments: Y.L., H.W.; drafting and critical revision of the manuscript: Y.L., X.F., H.W. All authors approved the final version of the manuscript.

RB/Ethical review board approval or patient consent/approval as a statement

Procedures for the collection and use of blood samples were approved by the Human Research Ethics Committee of the First Affiliated Hospital of Guangxi Medical University, and all subjects provided informed consent. All animal experiments were carried out with the approval of the Ethical Committee of Guangxi Medical University.

Data available on request from the authors

The data that support the findings of this study are available from the corresponding author, [X.F] and [H.W], upon reasonable request.

Declaration of Competing Interest

The authors declare no competing interests.

Acknowledgments

This work was funded by the National Natural Science Foundation of China (grant numbers 81960055), the Natural Science Foundation of Guangxi Province of China (grant number 2017GXNSFBA198045 and 2018GXNSFAA281217), and the Educational Commission of Guangxi Province of China (grant number 2018KY0107).

Supplementary materials

Supplementary material associated with this article can be found, in the online version, at doi:10.1016/j.tranon.2022.101424.

References

[1] G. Lepennetier, Z. Hracsko, M. Unger, M. Van Griensven, V. Grummel, M. Krumbholz, et al., Cytokine and immune cell profiling in the cerebrospinal fluid of patients with neuro-inflammatory diseases, J. Neuroinflammation 16 (1) (2019) 219, https://doi.org/10.1186/s12974-019-1601-6. PubMed PMID: 31727097; PubMed Central PMCID: PMCPMC6857241.

[2] Z. Zareen, T. Strickland, V.M. Eneaney, L.A. Kelly, D. McDonald, D. Sweetman, et al., Cytokine dysregulation persists in childhood post neonatal encephalopathy, BMC Neurol. 20 (1) (2020) 115, https://doi.org/10.1186/s12883-020-01656-w. PubMed PMID: 32228505.

[3] A. Comes, E. Di Carlo, P. Musiani, O. Rosso, R. Meazza, C. Chiodoni, et al., IFN-gamma-independent synergistic effects of IL-12 and IL-15 induce anti-tumor immune responses in syngeneic mice, Eur. J. Immunol. 32 (7) (2002) 1914–1923, https://doi.org/10.1002/1521-4141(200207)32:7.1914::AID-IMMU1914.3.0.CO;2-P. Epub 2002/07/13PubMed PMID: 12115611.

[4] T.A. Fehniger, M.A. Cooper, M.A. Caligiuri, Interleukin-2 and interleukin-15: immunotherapy for cancer, Cytokine Growth Factor Rev. 13 (2) (2002) 169–183, https://doi.org/10.1016/s1359-6101(01)00021-1. Epub 2002/03/20PubMed PMID: 11900992.

[5] A. Ma, R. Koka, P. Burkett, Diverse functions of IL-2, IL-15, and IL-7 in lymphoid homeostasis, Annu. Rev. Immunol. 24 (2006) 657–679, https://doi.org/10.1146/annurev.immunol.24.021605.090727. Epub 2006/03/23PubMed PMID: 16551262.

[6] M.C. Sneller, W.C. Kopp, K.J. Engelke, J.L. Yovandich, S.P. Creekmore, T. A. Waldmann, et al., IL-15 administered by continuous infusion to rhesus macaques induces massive expansion of CD8+ T effector memory population in peripheral blood, Blood 118 (26) (2011) 6845–6848, https://doi.org/10.1182/blood-2011-09-377804. Epub 2011/11/10PubMed PMID: 22067383; PubMed Central PMCID: PMCPMC3245206.

[7] M. Zhang, B. Wen, O.M. Anton, Z. Yao, S. Dubois, W. Ju, et al., IL-15 enhanced antibody-dependent cellular cytotoxicity mediated by NK cells and macrophages, Proc. Natl. Acad. Sci. U. S. A. 115 (46) (2018) E10915–E10E24, https://doi.org/10.1073/pnas.1811615115. Epub 2018/10/31PubMed PMID: 30373815; PubMed Central PMCID: PMCPMC6243244.

[8] T.A. Stoklasek, K.S. Schluns, L. Lefrancois, Combined IL-15/IL-15Ralpha immunotherapy maximizes IL-15 activity *in vivo*, J. Immunol. 177 (9) (2006) 6072–6080, https://doi.org/10.4049/jimmunol.177.9.6072. Epub 2006/10/24PubMed PMID: 17056533; PubMed Central PMCID: PMCPMC2847275.

[9] H. Kobayashi, J.A. Carrasquillo, C.H. Paik, T.A. Waldmann, Y. Tagaya, Differences of biodistribution, pharmacokinetics, and tumor targeting between interleukins 2 and 15, Cancer Res. 60 (13) (2000) 3577–3583. Epub 2000/07/26. PubMed PMID: 10910071.

[10] K.C. Conlon, E. Lugli, H.C. Welles, S.A. Rosenberg, A.T. Fojo, J.C. Morris, et al., Redistribution, hyperproliferation, activation of natural killer cells and CD8 T cells, and cytokine production during first-in-human clinical trial of recombinant human interleukin-15 in patients with cancer, J. Clin. Oncol. 33 (1) (2015) 74–82, https://doi.org/10.1200/JCO.2014.57.3329. Epub 2014/11/19PubMed PMID: 25403209; PubMed Central PMCID: PMCPMC4268254.

[11] J.U. Schmohl, M. Felices, E. Taras, J.S. Miller, D.A. Vallera, Enhanced ADCC and NK cell activation of an anticarcinoma bispecific antibody by genetic insertion of a modified IL-15 cross-linker, Mol. Ther. 24 (7) (2016) 1312–1322, https://doi.org/10.1038/mt.2016.88. Epub 2016/05/10PubMed PMID: 27157665; PubMed Central PMCID: PMCPMC5088765.

[12] U.S. Arvindam, P.M.M. van Hauten, D. Schirm, N. Schaap, W. Hobo, B.R. Blazar, et al., A trispecific killer engager molecule against CLEC12A effectively induces NK-cell mediated killing of AML cells, Leukemia 35 (6) (2021) 1586–1596, https://doi.org/10.1038/s41375-020-01065-5. Epub 2020/10/25PubMed PMID: 33097838; PubMed Central PMCID: PMCPMC8189652.

[13] S. Chen, Q. Huang, J. Liu, J. Xing, N. Zhang, Y. Liu, et al., A targeted IL-15 fusion protein with potent anti-tumor activity, Cancer Biol. Ther. 16 (9) (2015) 1415–1421, https://doi.org/10.1080/15384047.2015.1071739. Epub 2015/07/16PubMed PMID: 26176990; PubMed Central PMCID: PMCPMC4622986.

[14] Y. Liu, Y. Wang, J. Xing, Y. Li, J. Liu, Z. Wang, A novel multifunctional anti-CEA-IL15 molecule displays potent antitumor activities, Drug Des. Devel. Ther. 12 (2018) 2645–2654, https://doi.org/10.2147/DDDT.S166373. PubMed PMID: 30214153; PubMed Central PMCID: PMCPMC6120566.

[15] R. Arriga, S. Caratelli, G. Lanzilli, A. Ottaviani, C. Cenciarelli, T. Sconocchia, et al., CD16-158-valine chimeric receptor T cells overcome the resistance of KRAS-mutated colorectal carcinoma cells to cetuximab, Int. J. Cancer 146 (9) (2020) 2531–2538, https://doi.org/10.1002/ijc.32618. Epub 2019/08/10PubMed PMID: 31396956.

[16] Y. Li, C. Zhou, J. Li, J. Liu, L. Lin, L. Li, et al., Single domain based bispecific antibody, Muc1-Bi-1, and its humanized form, Muc1-Bi-2, induce potent cancer cell killing in muc1 positive tumor cells, PLoS ONE 13 (1) (2018), e0191024, https://doi.org/10.1371/journal.pone.0191024. Epub 2018/01/23PubMed PMID: 29357376; PubMed Central PMCID: PMCPMC5777659.

[17] Y. Zhao, Y. Li, X. Wu, L. Li, J. Liu, Y. Wang, et al., Identification of anti-CD16a single domain antibodies and their application in bispecific antibodies, Cancer Biol. Ther. 21 (1) (2020) 72–80, https://doi.org/10.1080/15384047.2019.1665953. Epub 2019/10/01PubMed PMID: 31564196; PubMed Central PMCID: PMCPMC7012161.

[18] C. Capuano, C. Pighi, S. Battella, D. De Federicis, R. Galandrini, G. Palmieri, Harnessing CD16-mediated NK cell functions to enhance therapeutic efficacy of tumor-targeting mAbs, Cancers (Basel) 13 (10) (2021), https://doi.org/10.3390/cancers13102500. Epub 2021/06/03PubMed PMID: 34065399; PubMed Central PMCID: PMCPMC8161310.

[19] F. Peng, L. Xiong, C. Peng, (-)-Sativan inhibits tumor development and regulates miR-200c/PD-L1 in triple negative breast cancer cells, Front. Pharmacol. 11 (2020) 251, https://doi.org/10.3389/fphar.2020.00251. PubMed PMID: 32231566; PubMed Central PMCID: PMCPMC7082844.

[20] M. Kocikowski, K. Dziubek, M. Parys, Hyperprogression under immune checkpoint-based immunotherapy-current understanding, the role of PD-1/PD-L1 tumour-intrinsic signalling, future directions and a potential largeanimal model, Cancers (Basel) 12 (4) (2020), https://doi.org/10.3390/cancers12040804. PubMed PMID: 32230745.

[21] H. Nagano, T. Watanabe, T. Togawa, K. Ohnishi, T. Kimura, A. Iida, et al., A rare case of moderately differentiated adenocarcinoma with PD-L1 overexpression and a heterogeneous LELC component in theascending Colon, OncoTargets Ther. 13 (2020) 791–801, https://doi.org/10.2147/OTT.S234945. PubMed PMID: 32095077; PubMed Central PMCID: PMCPMC6995307.

[22] E. Miyawaki, H. Murakami, K. Mori, N. Mamesaya, T. Kawamura, H. Kobayashi, et al., PD-L1 expression and response to pembrolizumab in patients with EGFR-mutant non-small cell lung cancer, Jpn. J. Clin. Oncol. (2020), https://doi.org/10.1093/jjco/hyaa033. PubMed PMID: 32211792.

[23] K. Nong, D. Zhang, C. Chen, Y. Yang, Y. Yang, S. Liu, et al., MicroRNA-519 inhibits hypoxia-induced tumorigenesis of pancreatic cancer by regulating immune checkpoint PD-L1, Oncol. Lett. 19 (2) (2020) 1427–1433, https://doi.org/10.3892/ol.2019.11234. PubMed PMID: 31966071; PubMed Central PMCID: PMCPMC6956369.

[24] J.A. Kagihara, M. Andress, J.R. Diamond, Nab-paclitaxel and atezolizumab for the treatment of PD-L1-positive, metastatic triple-negative breast cancer: review and future directions, Expert Rev. Precis. Med. Drug Dev. 5 (2) (2020) 59–65, https://doi.org/10.1080/23808993.2020.1730694. PubMed PMID: 32190733; PubMed Central PMCID: PMCPMC7080186.

[25] A. Farkkila, D.C. Gulhan, J. Casado, C.A. Jacobson, H. Nguyen, B. Kochupurakkal, et al., Immunogenomic profiling determines responses to combined PARP and PD-1 inhibition in ovarian cancer, Nat. Commun. 11 (1) (2020) 1459, https://doi.org/10.1038/s41467-020-15315-8. PubMed PMID: 32193378; PubMed Central PMCID: PMCPMC7081234.

[26] D. Yu, X. Liu, G. Han, Y. Liu, X. Zhao, D. Wang, et al., The let-7 family of microRNAs suppresses immune evasion in head and neck squamous cell carcinoma by promoting PD-L1 degradation, Cell Commun. Signal 17 (1) (2019) 173, https://doi.org/10.1186/s12964-019-0490-8. PubMed PMID: 31881947; PubMed Central PMCID: PMCPMC6935121.

[27] S.A. Gondhowiardjo, Adham A.M. Handoko, L. Rachmadi, H. Kodrat, D.L. Tobing, et al., Tumor microenvironment predicts local tumor extensiveness in PD-L1 positive nasopharyngeal cancer, PLoS ONE 15 (3) (2020), e0230449, https://doi.org/10.1371/journal.pone.0230449. PubMed PMID: 32191754; PubMed Central PMCID: PMCPMC7082005.

[28] B.H. Chamseddin, E.E. Lee, J. Kim, X. Zhan, R. Yang, K.M. Murphy, et al., Assessment of circularized E7 RNA, GLUT1, and PD-L1 in anal squamous cell carcinoma, Oncotarget 10 (57) (2019) 5958–5969, https://doi.org/10.18632/oncotarget.27234. PubMed PMID: 31666927; PubMed Central PMCID: PMCPMC6800260.

[29] A.J. Schoenfeld, H. Rizvi, C. Bandlamudi, J.L. Sauter, W.D. Travis, N. Rekhtman, et al., Clinical and molecular correlates of PD-L1 expression in patients with lung adenocarcinomas, Ann. Oncol. (2020), https://doi.org/10.1016/j.annonc.2020.01.065. PubMed PMID: 32178965.

[30] M. Ilie, V. Hofman, M. Dietel, J.C. Soria, P. Hofman, Assessment of the PD-L1 status by immunohistochemistry: challenges and perspectives for therapeutic strategies in lung cancer patients, Virchows Arch. 468 (5) (2016) 511–525, https://doi.org/10.1007/s00428-016-1910-4. PubMed PMID: 26915032.

[31] M. Kijanka, B. Dorresteijn, S. Oliveira, P.M. van Bergen en Henegouwen, Nanobody-based cancer therapy of solid tumors, Nanomedicine (Lond) 10 (1) (2015) 161–174, https://doi.org/10.2217/nnm.14.178. Epub 2015/01/20PubMed PMID: 25597775.

[32] C. Hamers-Casterman, T. Atarhouch, S. Muyldermans, G. Robinson, C. Hamers, E. B. Songa, et al., Naturally occurring antibodies devoid of light chains, Nature 363

(6428) (1993) 446–448, https://doi.org/10.1038/363446a0. Epub 1993/06/03PubMed PMID: 8502296.
[33] S. Muyldermans, Nanobodies: natural single-domain antibodies, Annu. Rev. Biochem. 82 (2013) 775–797, https://doi.org/10.1146/annurev-biochem-063011-092449. Epub 2013/03/19PubMed PMID: 23495938.
[34] R.H. van der Linden, L.G. Frenken, B. de Geus, M.M. Harmsen, R.C. Ruuls, W. Stok, et al., Comparison of physical chemical properties of llama VHH antibody fragments and mouse monoclonal antibodies, Biochim. Biophys. Acta 1431 (1) (1999) 37–46, https://doi.org/10.1016/s0167-4838(99)00030-8. Epub 1999/04/21PubMed PMID: 10209277.
[35] C.S. Stewart, C.R. MacKenzie, J.C. Hall, Isolation, characterization and pentamerization of alpha-cobrotoxin specific single-domain antibodies from a naive phage display library: preliminary findings for antivenom development, Toxicon 49 (5) (2007) 699–709, https://doi.org/10.1016/j.toxicon.2006.11.023. Epub 2007/01/30PubMed PMID: 17257638.
[36] M.S. Zambrano-Mila, K.E. Sanchez Blacio, N. Santiago Vispo, Peptide phage display: molecular principles and biomedical applications, Ther. Innov. Regul. Sci. (2019), 2168479019837624, https://doi.org/10.1177/2168479019837624. PubMed PMID: 30922115.
[37] S. Mimmi, D. Maisano, I. Quinto, E. Iaccino, Phage display: an overview in context to drug discovery, Trends Pharmacol. Sci. 40 (2) (2019) 87–91, https://doi.org/10.1016/j.tips.2018.12.005. PubMed PMID: 30606501.
[38] P.L. Campbell, R.L. Duda, J. Nassur, J.F. Conway, A. Huet, Mobile loops and electrostatic interactions maintain the flexible tail tube of bacteriophage lambda, J. Mol. Biol. 432 (2) (2020) 384–395, https://doi.org/10.1016/j.jmb.2019.10.031. PubMed PMID: 31711962.
[39] E. Beghetto, N. Gargano, Whole-genome phage display libraries: apowerful tool for antigen discovery, Methods Mol. Biol. 2024 (2019) 181–198, https://doi.org/10.1007/978-1-4939-9597-4_11. PubMed PMID: 31364050.
[40] A. Arab, J. Nicastro, R. Slavcev, A. Razazan, N. Barati, A.R. Nikpoor, et al., Lambda phage nanoparticles displaying Her2-derived E75 peptide induce effective E75-CD8(+) T response, Immunol. Res. 66 (1) (2018) 200–206, https://doi.org/10.1007/s12026-017-8969-0. PubMed PMID: 29143917.
[41] X. Wu, S. Chen, L. Lin, J. Liu, Y. Wang, Y. Li, et al., A single domain-based anti-Her2 antibody has potent antitumor activities, Transl. Oncol. 11 (2) (2018) 366–373, https://doi.org/10.1016/j.tranon.2018.01.024. PubMed PMID: 29455083; PubMed Central PMCID: PMCPMC5852409.
[42] E. Mortier, A. Quemener, P. Vusio, I. Lorenzen, Y. Boublik, J. Grotzinger, et al., Soluble interleukin-15 receptor alpha (IL-15R alpha)-sushi as a selective and potent agonist of IL-15 action through IL-15R beta/gamma. Hyperagonist IL-15 x IL-15R alpha fusion proteins, J. Biol. Chem. 281 (3) (2006) 1612–1619, https://doi.org/10.1074/jbc.M508624200. Epub 2005/11/15PubMed PMID: 16284400.
[43] Y. Li, Y. Zhu, S. Feng, Y. Ishida, T.P. Chiu, T. Saito, et al., Macrophages activated by hepatitis B virus have distinct metabolic profiles and suppress the virus via IL-1beta to downregulate PPARalpha and FOXO3, Cell Rep. 38 (4) (2022), 110284, https://doi.org/10.1016/j.celrep.2021.110284. Epub 2022/01/27PubMed PMID: 35081341; PubMed Central PMCID: PMCPMC8830375.
[44] J. Huang, Y. Li, Z. Jiang, L. Wu, Y. Liu, S. Ma, et al., IL-1beta promotes hypoxic vascular endothelial cell proliferation through the miR-24-3p/NKAP/NF-kappaB axis, Biosci. Rep. 42 (1) (2022), https://doi.org/10.1042/BSR20212062. Epub 2022/01/11PubMed PMID: 35005769; PubMed Central PMCID: PMCPMC8766822.
[45] Y. Li, L. Yan, W. Zhang, N. Hu, W. Chen, H. Wang, et al., MicroRNA-21 inhibits platelet-derived growth factor-induced human aortic vascular smooth muscle cell proliferation and migration through targeting activator protein-1, Am. J. Transl. Res. 6 (5) (2014) 507–516. Epub 2014/11/02. PubMed PMID: 25360215; PubMed Central PMCID: PMCPMC4212925.
[46] Y. Li, J. Huang, Z. Jiang, Y. Zhong, M. Xia, H. Wang, et al., MicroRNA-145 regulates platelet-derived growth factor-induced human aortic vascular smooth muscle cell proliferation and migration by targeting CD40, Am. J. Transl. Res. 8 (4) (2016) 1813–1825. Epub 2016/05/18. PubMed PMID: 27186305; PubMed Central PMCID: PMCPMC4859910.
[47] J. Liu, X. Wu, L. Lin, H. Pan, Y. Wang, Y. Li, et al., Bp-Bs, a novel T-cell engaging bispecific antibody with biparatopic Her2 binding, has potent anti-tumor Activities, Mol. Ther. Oncolytics 14 (2019) 66–73, https://doi.org/10.1016/j.omto.2019.03.009. Epub 2019/04/26PubMed PMID: 31020038; PubMed Central PMCID: PMCPMC6475711.
[48] P. Pandiyan, X.P. Yang, S.S. Saravanamuthu, L.X. Zheng, S. Ishihara, J.J. O'Shea, et al., The role of IL-15 in activating STAT5 and fine-tuning IL-17A production in CD_4 T lymphocytes, J. Immunol. 189 (9) (2012) 4237–4246, https://doi.org/10.4049/jimmunol.1201476. PubMed PMID: WOS:000310200600009.
[49] J. Guo, Y. Liang, D. Xue, J. Shen, Y. Cai, J. Zhu, et al., Tumor-conditional IL-15 pro-cytokine reactivates anti-tumor immunity with limited toxicity, Cell Res. 31 (11) (2021) 1190–1198, https://doi.org/10.1038/s41422-021-00543-4. Epub 2021/08/12PubMed PMID: 34376814; PubMed Central PMCID: PMCPMC8563767.
[50] J. Huang, Q. Weng, Y. Shi, W. Mao, Z. Zhao, R. Wu, et al., MicroRNA-155-5p suppresses PD-L1 expression in lung adenocarcinoma, FEBS Open Bio (2020), https://doi.org/10.1002/2211-5463.12853. PubMed PMID: 32237066.
[51] Y. Jiang, X. Zhao, J. Fu, H. Wang, Progress and challenges in precise treatment of tumors with PD-1/PD-L1 blockade, Front. Immunol. 11 (2020) 339, https://doi.org/10.3389/fimmu.2020.00339. PubMed PMID: 32226426; PubMed Central PMCID: PMCPMC7080697.
[52] M.E. Keir, Y.E. Latchman, G.J. Freeman, A.H. Sharpe, Programmed death-1 (PD-1): PD-ligand 1 interactions inhibit TCR-mediated positive selection of thymocytes, J. Immunol. 175 (11) (2005) 7372–7379, https://doi.org/10.4049/jimmunol.175.11.7372. PubMed PMID: 16301644; PubMed Central PMCID: PMCPMC2779139.
[53] D.Y. Kang, N. Sp, E.S. Jo, A. Rugamba, D.Y. Hong, H.G. Lee, et al., The inhibitory mechanisms of tumor PD-L1 expression by natural bioactive gallic acid in non-small-cell lung cancer (NSCLC) cells, Cancers (Basel) 12 (3) (2020), https://doi.org/10.3390/cancers12030727. PubMed PMID: 32204508.
[54] M. Herfs, P. Roncarati, B. Koopmansch, O. Peulen, D. Bruyere, A. Lebeau, et al., A dualistic model of primary anal canal adenocarcinoma with distinct cellular origins, etiologies, inflammatory microenvironments and mutational signatures: implications for personalised medicine, Br. J. Cancer 118 (10) (2018) 1302–1312, https://doi.org/10.1038/s41416-018-0049-2. PubMed PMID: 29700411; PubMed Central PMCID: PMCPMC5959925.
[55] S. Outh-Gauer, A. Morini, E. Tartour, C. Lepine, A.C. Jung, C. Badoual, The microenvironment of head and neck cancers: papillomavirus involvement and potential Impact of immunomodulatory treatments, Head Neck Pathol. (2020), https://doi.org/10.1007/s12105-020-01147-x. PubMed PMID: 32124416.
[56] J.H. Rasmussen, G. Lelkaitis, K. Hakansson, I.R. Vogelius, H.H. Johannesen, B. M. Fischer, et al., Intratumor heterogeneity of PD-L1 expression in head and neck squamous cell carcinoma, Br. J. Cancer 120 (10) (2019) 1003–1006, https://doi.org/10.1038/s41416-019-0449-y. PubMed PMID: 30967647; PubMed Central PMCID: PMCPMC6734649.
[57] X. Yang, J. Shi, X. Chen, Y. Jiang, H. Zhao, Efficacy of cabozantinib and nivolumab in treating hepatocellular carcinoma with RET amplification, high tumor mutational burden, and PD-L1 expression, Oncologist (2020), https://doi.org/10.1634/theoncologist.2019-0563. PubMed PMID: 32100934.
[58] S.M. Swain, J. Baselga, S.B. Kim, J. Ro, V. Semiglazov, M. Campone, et al., Pertuzumab, trastuzumab, and docetaxel in Her2-positive metastatic breast cancer, N. Engl. J. Med. 372 (8) (2015) 724–734, https://doi.org/10.1056/NEJMoa1413513. Epub 2015/02/19PubMed PMID: 25693012; PubMed Central PMCID: PMCPMC5584549.
[59] S.M. Swain, S.B. Kim, J. Cortes, J. Ro, V. Semiglazov, M. Campone, et al., Pertuzumab, trastuzumab, and docetaxel for Her2-positive metastatic breast cancer (CLEOPATRA study): overall survival results from a randomised, double-blind, placebo-controlled, phase 3 study, Lancet Oncol. 14 (6) (2013) 461–471, https://doi.org/10.1016/S1470-2045(13)70130-X. Epub 2013/04/23PubMed PMID: 23602601; PubMed Central PMCID: PMCPMC4076842.